Feeding H_2-admixtures to domestic condensing boilers: numerical simulations of combustion and pollutant formation in multi-hole burners

Rachele Lamioni[a,*], Cristiana Bronzoni[b], Marco Folli[b], Leonardo Tognotti[a], Chiara Galletti[a]

[a] *Dipartimento di Ingegneria Civile e Industriale, Università di Pisa, 56126 Pisa, Italy*
[b] *Ricerca & Sviluppo - Laboratorio Sviluppo Prodotti, Immergas S.p.A. , Brescello (RE) - Italy*

Abstract

Hydrogen can be produced through electrolysis from excess wind and solar power. Then, its injection into the natural gas network allows mitigating the challenges posed by the variability and intermittency of renewables, by exploiting the existing infrastructure for storage and distribution. However, the addition of hydrogen to natural gas affects gas properties; hence we need to ensure the safe and efficient operation of existing end-user equipment, such as domestic burners and boilers. This work intends to investigate the effect of H_2 addition on the combustion process and pollutant emissions in domestic condensing boilers. To this purpose, 3-dimensional numerical simulations of multi-hole geometries mimicking perforated burners, typically encountered in such appliances, are performed by using detailed kinetics and taking into account different hole-to-hole distances. Indeed, since the burner holes are located very close to each other, the neighbor premixed flames can interact,

*Corresponding author
Email address: rachele.lamioni@dici.unipi.it (Rachele Lamioni)

thus differing from single flame behavior. The impact of H_2 on the operating conditions, i.e. equivalence ratio and thermal load, is preliminarily evaluated to ensure that the numerical model closely emulates the practical situation we expect from the fuel composition change. Anticipation of the reaction zone occurs with H_2-admixtures, while the downstream temperature decreases because the boiler naturally shifts towards leaner conditions and smaller thermal loads when adding H_2 to natural gas. This behavior has a positive impact on pollutant emissions as the NO thermal formation route is suppressed in a larger measure than the increase of the NNH-intermediate contribution.
Keywords: Hydrogen, Domestic appliances, Laminar flames, Low emission, CFD

1. Introduction

Hydrogen is thought to be a key player for our transition to a decarbonized energy system. Indeed, power-to-gas plants produce green hydrogen in a clean and sustainable manner through electrolysis employing wind or solar energy as a power source and water [1]. Then, hydrogen can be effectively stored and distributed via the existing natural gas grid, thus making use of the large available infrastructure asset [2, 3]. Hence, such integration of power-to-gas with the natural gas network allows mitigating the challenges posed by the variability and intermittency of renewables, by facing the problem of storing and transporting the overproduction of energy. For instance, it has been estimated that 25 TWh of hydrogen could be blended into the European natural gas network by 2030 and that hydrogen could provide about

18% of the energy required for domestic heating in EU by 2050 [4]. This is extremely important if we think that the residential sector is responsible for approximately 30% of the total European energy consumption and it is projected to keep its share up to 2050 with the most significant part (65% in 2010, projected to be still 58% in 2050) being employed for heating. Moreover, the share of gaseous fuels is not expected to vary significantly up to 2050 [5].

Such expectations on hydrogen as a key enabler for the decarbonization of domestic heating should however face the fact that hydrogen is a very peculiar fuel, which shows much higher reactivity and adiabatic flame temperature than other fuels. This behavior opens a number of issues, related to the impact of its use on the maximum temperature, pollutant emissions as well as on heat exchange in domestic appliances. Besides, the much lower density of hydrogen in comparison with existing fuels would probably ask for a re-design of the burner. Hence, significant challenges may arise for the safe and efficient operation of existing end-user equipment, such as domestic burners and boilers. Even though maximum hydrogen fractions, up to 20% are foreseen for domestic applications, there is little proof of the adequate performance of such systems when adding hydrogen [6].

In this framework, the attention is towards modern condensing boilers as their share is growing significantly due to the increased efficiency with respect to non-condensing devices. Indeed, condensing boilers recover the latent heat of the water vapor in the flue gas by condensation, as the flue gas temperature is in the range $T = 30 \div 60^{\circ}$ C depending on the boiler duty and water-temperature needs. Hence, the boiler efficiency, which is usually

referred to the lower heating value (LHV), i.e. it is the useful delivered heat to LHV ratio, exceeds 100%, reaching values up to 115% [7]. This behavior yet allows for a great reduction of fuel consumption and associated CO_2 emissions than traditional non-condensing boilers. However, a chance for further decarbonization may be opened through feeding these appliances with H_2-admixtures.

Domestic condensing boilers are usually equipped with cylindrical or flat perforated burners which inject a premixed mixture into the combustion chamber. The major characteristic of such burners is to generate uniform temperature with flames that are short enough to accommodate in compact volumes [6]. Indeed, in condensing boilers, the distance between the heat exchanger and the burner is reduced with respect to conventional ones.

The burner design stems mainly from the experience of the manufacturers as well as from trial-and-error procedures [8]. Indeed, the impact of this design on the energy conversion process has not been an issue so far, with most of the attention being devoted at the improvement of the boiler efficiency and the optimization of the heat exchange.

However, the upcoming variations in the gas composition due to the injection of green hydrogen in the gas network could lead to changes in the flames which may ultimately impact emissivity, boiler efficiency as well as pollutants. Hence a deeper comprehension of the reactive flow in domestic boilers is required to better address these variations in the gas composition and devise strategies for the optimal use of green hydrogen in domestic condensing boilers.

Some experimental investigations analyzed the performance of perforated

burners in different operating conditions. Lee et al. [9] analyzed flame stability and emissions of pollutants, i.e. NOx and CO, from a perforated cylindrical burner fed with methane. The authors observed that the optimal equivalence ratio was $0.70 < \phi < 0.75$. Najarnikoo et al. [10] confirmed the above results as they indicated the optimal conditions for $0.70 < \phi < 0.73$ ensuring a stable blue flame. Schiro et al. [8] investigated different cylindrical premixed burners, i.e. perforated and with metal fibers, fed with different gases. The authors showed how CO emissions increase with thermal load, as the residence time in the chamber decreases. As for NOx, metal fiber burners were found to provide significantly lower NOx than steel ones. Soltanian et al. [11] used chemiluminescence to investigate OH* and CO2* emissions from a multi-hole cylindrical burner. The authors observed that the heat transfer rate, which is directly related to OH* and CO2*, was maximized for $\phi \approx 0.82$. Ding et al. [12] showed that OH* chemiluminescence signals could be used for sensing the equivalence ratio in domestic boilers also in case of variable fuel composition, including H_2 admixtures. Burbano et al. [13] analyzed the effects of hydrogen addition to methane on the flame structure and CO emissions in single- and drilled-port atmospheric burner. The height of the blue cone was observed to diminish with hydrogen in the single-port burner because of the increase of the laminar burning velocity. In the drilled-port burner, CO emissions were found to decrease with hydrogen addition when the primary air ratio was kept constant.

Further and significant insight into the impact of the burner design on the energy conversion in domestic condensing boilers could be achieved with the application of Computational Fluid Dynamics (CFD) techniques, which have

grown considerably in the last decades along with the rapid development of computational power. Indeed, CFD allows solving the equations which govern the fluid dynamics, chemical reactions and associated phenomena in complex geometrical domains and taking into account the mixture properties. This may be used firstly to support and explain the experimental evidence, with the ultimate goal to provide a novel tool to improve the know-how and the design of premixed perforated burners. This many also help to address the issues related to the much lower density of hydrogen with respect to natural gas.

So far CFD has been applied to condensing boilers mainly to address the problem of gas distribution and mixing upstream of the burner and only a few works have dealt with the simulation of the reactive flow. Zhao et al. [14] investigated numerically, though non-reactive CFD simulations, the influence of geometrical parameters, i.e. nozzle exit position and nozzle diameter, on the gas distribution from a perforated cylindrical burner. Zhang et al. [15] used CFD to optimize the gas mixing system of a premixed burner. They also showed experimentally that the uniformity at the outlet of the mixing system affects strongly the emission of NOx and CO. Saberi Moghaddam et al. [16] carried out numerical simulations of a multi-hole flat flame to show how the presence of a distribution mesh could improve the flow uniformity among the burner holes.

Hassan et al. [17] developed a 2-dimensional CFD model based on the partially premixed and equilibrium chemistry calculations to simulate the combustion process taking place in the combustion chamber of a domestic boiler equipped with a perforated cylindrical burner. The numerical results

indicated that the main sources for CO and NO emissions are the dissociation of CO_2 and thermal NO mechanisms, respectively. Altay et al., [18] performed 2-dimensional CFD simulations of laminar premixed methane-air flames emulating a single hole of a flat perforated burner and including the effect of the heat exchange with the burner plate. The authors observed that this heat exchange affects strongly the flame morphology. Kedia and Ghoniem [19] carried out 2-dimensional simulations with detailed kinetics to investigate the blow-off conditions of a laminar premixed flame issuing from a multi-hole burner. The 3-dimensional simulations of laminar premixed propane-air flames from a flat perforated burner by Jothin et al. [20] indicated that the flame stand-off distance augments with increasing the thermal conductivity of the burner plate. Veetil et al. [21] analyzed numerically the effect of hole configuration and hole-to-hole distance on the flame structure of steady laminar premixed methane-air flames issuing from a flat perforated plate. Lamioni et al. [22] and Attili et al. [23] estimated numerically the effect of the pressure on the flame structure of laminar premixed methane-air flames in the slot configuration.

Hinrichs et al. [24] carried out numerical simulations with detailed chemistry to shed light on the main pathways to pollutant emissions, i.e. NO e and CO, is a condensing boiler. Their model was limited to a single hole of a perforated cylindrical burner and equipped with a region emulating the heat exchange. The authors found that the CO concentration in the cooled flue gases was significantly larger than the chemical equilibrium one. This behavior was imputed to the rapid quenching, triggered by the fast depletion of OH radicals, of CO oxidation reactions.

Although the application of CFD for the design of burners for domestic heating is still under development, we believe that the above investigations prove the potentiality of mathematical models in helping to understand the effect of key parameters as well as operating conditions. In this scenario, the present work [1] aims at assessing the impact of H_2 on domestic condensing boilers by carrying out 3-D numerical simulations of multi-hole flames issuing from perforated burners. To this purpose, we intend to adopt the real operating conditions occurring with H_2. Hence, preliminary, analysis is carried out to determine these conditions, i.e. thermal input and equivalence ratio, of domestic condensing boilers fed with mixtures having different H_2 contents. Besides, special attention is devoted to the interaction between flames as one of the main features of the perforated burners is that the holes are positioned very close to each other.

2. Test case

An example of a perforated cylindrical burner is provided in Figure 1(a). Here we notice the presence of both circular holes and slits; however, some burners exhibit only circular holes [9]. In this work we focus on the pattern of circular holes as reported in Figure 1(b). The holes have a diameter D and their centers are placed at the vertices of a $R \times 1.1R$ rectangle. This geometry closely emulates the typical patterns of practical burners.
To investigate the effect of flame interaction, the distance between the holes was varied by using three different R/D ratios, i.e. $R/D = 1.5, 1.75$ and 2.

[1] The short version of the paper was presented at 100%RES, October 29-30, Pisa. This paper is a substantial extension of the short version of the conference paper.

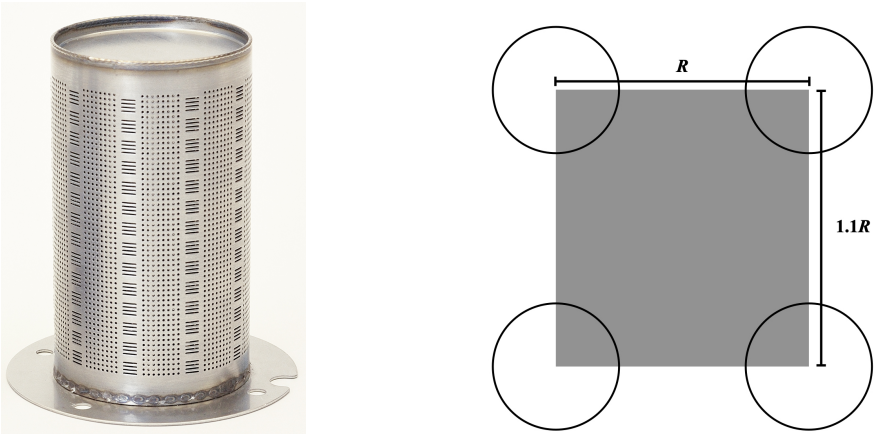

(a) (b)

Figure 1: Typical cylindrical burner (a) and pattern of holes (b).

3. Numerical model

Preliminary, 1-D freely propagating flames are simulated using openSmoke-suite [25] to analyse the flame structure. Subsequently a 3-D model with CFD is developed to gain insight into the effect of the geometrical configuration on the interaction between the flames.
In both 1-D and CFD models we employed the `GRI3.0` mechanism, including 53 reactive chemical species and 325 elementary reactions [26].

3.1. Physical model

The problem is described through the conservation of mass, momentum, energy, and the transport/reaction of chemical species. In steady-state conditions and for the low-Mach approximation the system of equations is:

$$\nabla \cdot (\rho \mathbf{v}) = 0 \tag{1}$$

$$\nabla \cdot (\rho \mathbf{v}\mathbf{v}) = \nabla p + \nabla \cdot (\bar{\tau}) \tag{2}$$

$$\nabla \cdot (\rho c_p T \mathbf{v}) = \mathbf{v} \cdot \nabla p + \nabla \cdot (k \nabla T) + \rho \left(\sum_1^N \mathcal{D}_i c_{p,i} \nabla Y_i \right) \cdot \nabla T - \sum_1^N h_i \omega_i + q_{rad} \tag{3}$$

$$\nabla \cdot (\rho Y_i \mathbf{v}) = -\rho \mathcal{D}_i \nabla^2 Y_i + \omega_i \tag{4}$$

where $\mathbf{v}$ is the velocity vector, $\bar{\tau}$ is the stress tensor, p is pressure, T is the temperature and Y_i is the mass fraction of the i-th chemical species. rho and k are the density and thermal conductivity, respectively, while h_i is the enthalpy of the i-th chemical species. $\mathcal{D}_i$ is the mass diffusivity of the i-th species in the mixture. Binary diffusion coefficients are firstly calculated following the kinetic theory and a modification of the Chapman–Enskog formula; then $\mathcal{D}_i$ is obtained by applying the Wilke's mixing rule. ω_i is the net rate of production or consumption of the i-th species due to chemical reaction, while q_{rad} is the energy source term associated to radiation.
It is worth noting that ω_i is calculated explicitly as we are in laminar conditions. As for radiation, the P1 model [27, 28] is applied along with the weighted-sum-of-gray-gases model with coefficients from Smith [29] to evaluate the spectral properties of the gaseous medium.

3.2. Computational domain and grid

The computational domain consists of four quarters of holes, as depicted in Figure 2, and was sufficiently long to enclose the whole flames, i.e. $L = 25D$, where L represents the longitudinal extension of the domain. In particular, we used the values of the laminar flame speed from the 1-D freely

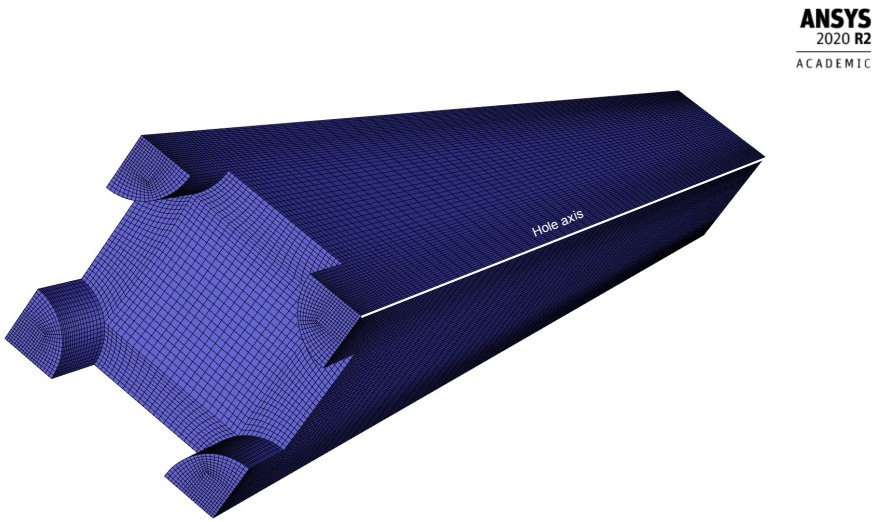

Figure 2: Computational grid for R_3 configuration with indication of the hole axis.

propagating flames to estimate the height of a typical Bunsen flame. Results indicated $L \approx 10D$ and $L \approx 12D$ for natural gas and the mixture with the highest H_2 content, respectively. Hence, to avoid boundary effects, we safely employed a domain that is more than twice longer, i.e. $L = 25D$.

Actually, the symmetries of the burner suggest that just a single quarter of hole can be considered; however, to better study the the flame interaction, four quarters of holes were taken into account.

A block-structured grid was generated by applying the O-grid strategy available in ICEM by ANSYS. The choice of the characteristic cell size in the reaction front region was guided by the preliminary 1-D simulations, carried out with the open-source code OPENSMOKE-SUITE [25], of freely propagating flames. In particular, at least 10 computational nodes were fitted in the thermal flame thickness, i.e., l_T, which was calculated by using the resulting

temperature profiles [30] as:

$$l_T = \frac{T_b - T_u}{\frac{\partial T}{\partial x}|_{max}} \tag{5}$$

where T_b and T_u are temperatures of the burnt and fresh gases, respectively and $\partial T/\partial x$ is the temperature gradient. A grid independence study was also preliminary carried out for one configuration, confirming the suitability of the above approach to determine the cell size in the flame front. The resulting number of cells is reported in Table 1 along with the domain extension for the three different configurations, i.e. the hole-to-hole distances R. A picture of one computational grid is provided in Figure 2.

Table 1: Dimension of the computational domain in units of hole diameter D for the three configurations. R represents the hole-to-hole distance and N_{cell} is the number of computational cells.

Case	R	Domain	N_{cell}
R_1	$1.5D$	$25D$x$1.5D$x$1.65D$	56000
R_2	$1.75D$	$25D$x$1.75D$x$1.9D$	64000
R_3	$2D$	$25D$x$2D$x$2.2D$	73000

3.3. Boundary conditions

We employ natural gas, i.e. G20 test gas, and two H_2-admixtures, i.e. G222 and H2NG gases, whose H_2 content is 23% and 50% by volume, respectively, as reported in Table 2: In the reference case, i.e. G20 test gas, we consider a thermal power of 25 kW and an equivalence ratio $\phi = 0.8$, which corresponds to optimal operating condition. Indeed such equivalence ratio is in agreement with indications from literature [11]. The equivalence

Table 2: Composition of the test gases, corresponding Wobbe index, thermal power and equivalence ratio.

test gas	H_2 [% by vol]	CH_4 [% by vol]	W [-]	P_{th} [kW]	$\phi[-]$
G20	0	100	53.5	25	0.8
G222	23	77	50.5	23.6	0.74
H2NG	50	50	47.0	22.0	0.67

ratios for the H_2 admixtures were determined following the procedure given by [31] regarding the interchangeability of gas mixtures in domestic appliances. We can write the equivalence ratio as a function of the stoichiometric air requirement, i.e. LdV, representing the volume of air required to oxidize one volume of fuel, as:

$$\phi = \frac{(F/A)}{(F/A)_{st}} = (F/A) \cdot Ldv \tag{6}$$

where F and A are the volumetric flow rates of the fuel and air, respectively, while the subscript st indicates the stoichiometric conditions.

If we change the fuel composition at constant supply pressure, the fuel volumetric flow rate F changes as

$$F \propto \frac{1}{\sqrt{\rho/\rho_0}} \tag{7}$$

with ρ_0 being the density of air at 0°C. Subsequently the thermal input also varies as:

$$P_{th} = F \cdot HHV \propto \frac{HHV}{\sqrt{\rho/\rho_0}} \propto W \tag{8}$$

where W is the Wobbe index. Table 2 lists the Wobbe indexes as estimated at 25°C and ambient pressure for the three mixtures and subsequently the

thermal power P_{th}.

At constant supply pressure, the pressure of the fuel entering the burner does not depend on composition. This behaviour implies that the momentum of the fuel jet is constant; hence the air flow rate, i.e. A, will also be constant, in burners which are equipped with a venturi to draw air [31]. Hence, by replacing the G20 gas with an H_2-admixtures, a shift in the equivalence ratio to smaller values naturally occurs, according to the following expression:

$$\Delta\phi = \phi_{H2adm} - \phi_{G20} = \phi_{G20} \left[\frac{Ldv_{G20}}{Ldv_{H2adm}} \cdot \sqrt{\frac{\rho_{G20}}{\rho_{H2adm}}} - 1 \right] \tag{9}$$

The estimated equivalence ratios for the H_2-admixtures are reported in Table 2. We notice how the H2NG mixture operates in leaner condition, i.e. with ϕ=0.67, with respect to the G20 test gas.

In the computational model, uniform velocity and uniform temperature of $T_u = 300$ K, were set at inlets, while a pressure outlet was imposed at the exit of the domain. Velocities were estimated from the F and A values, and considering the total area of the holes of a typical cylindrical burner. In all cases, the flow is fully laminar as also pointed out in other works in literature [32]. The Reynolds number estimated using the hole diameter and the mixture properties at the inlet temperature, i.e. T_u, is $Re = 55$ for the G20 gas test.

Symmetry conditions were assigned to the domain sides. A temperature $T_w = 750$ K was prescribed at the burner plate, to take into account of the heat exchange with the gas mixture. Such plate temperature was estimated from experimental data available for this type of burner and is in agreement with other works in literature [11, 12, 33].

3.4. Solution methodology

The above set of equations was solved with the pressure-based coupled algorithm available in ANSYS- FLUENT 19.2 [34] using a central difference scheme for diffusion terms and second-order upwind scheme for convection terms. Chemistry integration was carried out using direct integration method. The fuel-oxidiser mixture is ignited by patching a region near to the inlet by setting a high temperature (2500 K). At convergence normalised residuals did not change with iterations and were all below 10^{-6}.

4. Results

4.1. Effect of the hole-to-hole distance

Figure 3 shows the temperature, CH_4, O_2 and OH mole fractions along the flame axis for the G20 gas, i.e. natural gas, as computed by the 1-D simulations of freely propagating flames and by the 3-D CFD simulations, the latter being carried out for different distances R between the burner holes.

Major species as CH_4 and O_2 mole fractions on the fresh and burnt sides, indicated a good agreement between 1-D and 3-D predictions, as well as with the literature [35], thus confirming also the accuracy of the reacting module available in the CFD code. Some differences are present in the flame front. This behavior indicates that the features included in the 3-D model, i.e. the presence of a burner plate, play a role. In particular, the 3-D model accounts for the heat exchange between the flame and plate; hence, here the temperature rise is anticipated with respect to the freely propagating flame. In addition, we observe that also the hole-to-hole distance has an impact

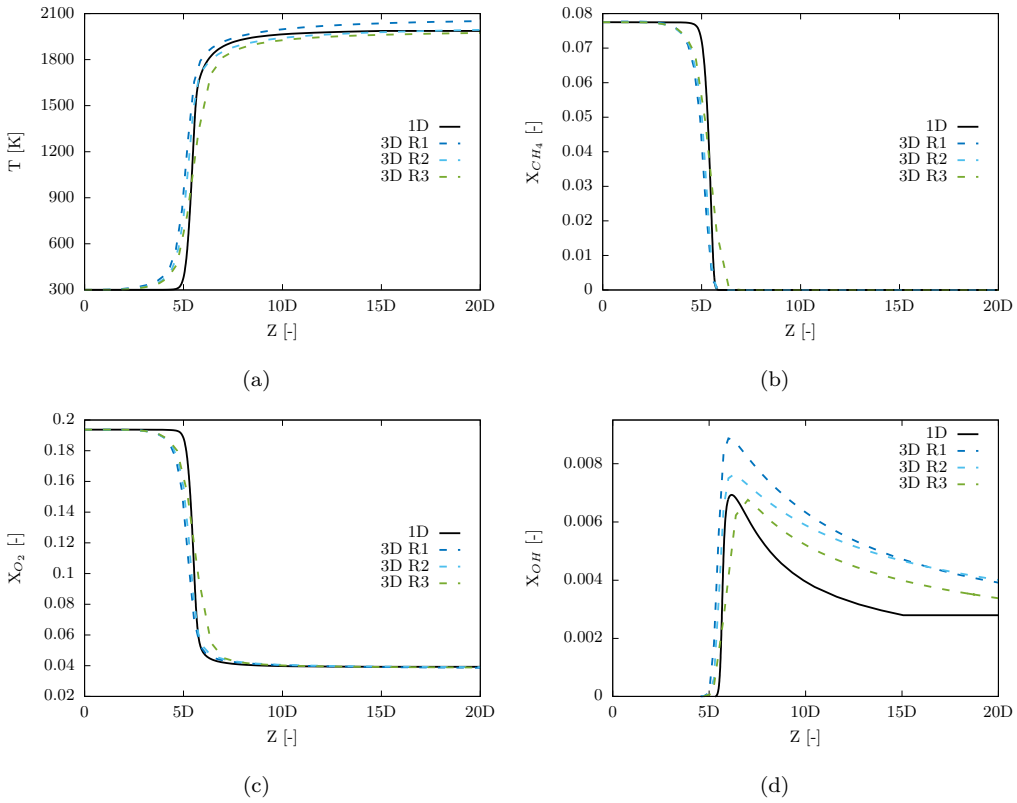

Figure 3: Profiles along the hole axis of (a) temperature, (b) CH_4, (c) O_2 and (d) add figure correctOH mole fraction predicted by the 1-D (solid lines) and 3-D (dashed lines) models. G20 gas.

on the thermo-chemical field, thus indicating that a flame in a group, for such distances, behaves differently than a single flame. Such differences are even more pronounced if we look at the OH concentration, which highlights significant discrepancies between the freely propagating flame and the 3-D model. Again, the hole-to-hole distance affects remarkably the OH levels. The strongest reaction zone, which is denoted by the highest values of the OH flame marker, occurs for the smallest R values, i.e. for the closest flames.

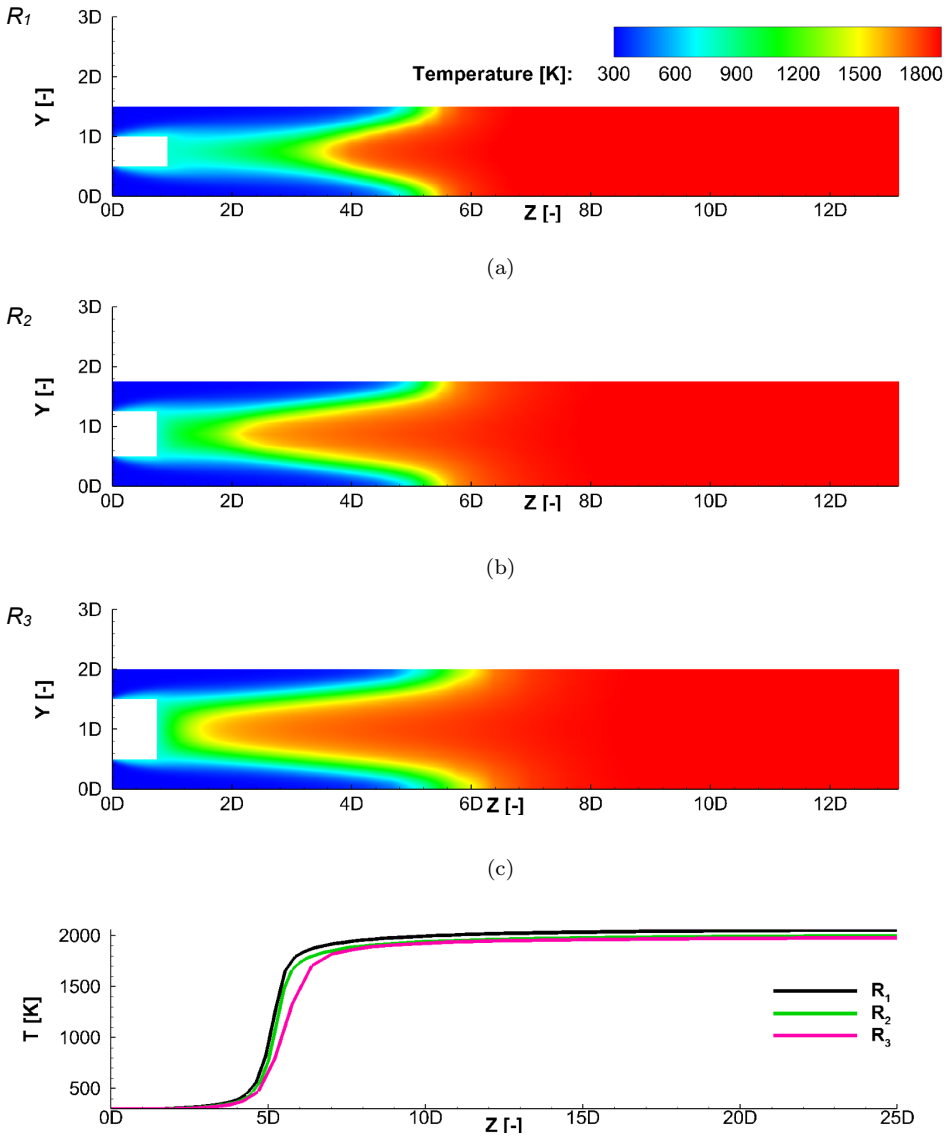

Figure 4: Temperature distribution in the longitudinal plane crossing the axes of two adjacent holes for (a) R_1, (b) R_2, (c) R_3 and (d) temperature profiles along the hole axis. G20 gas.

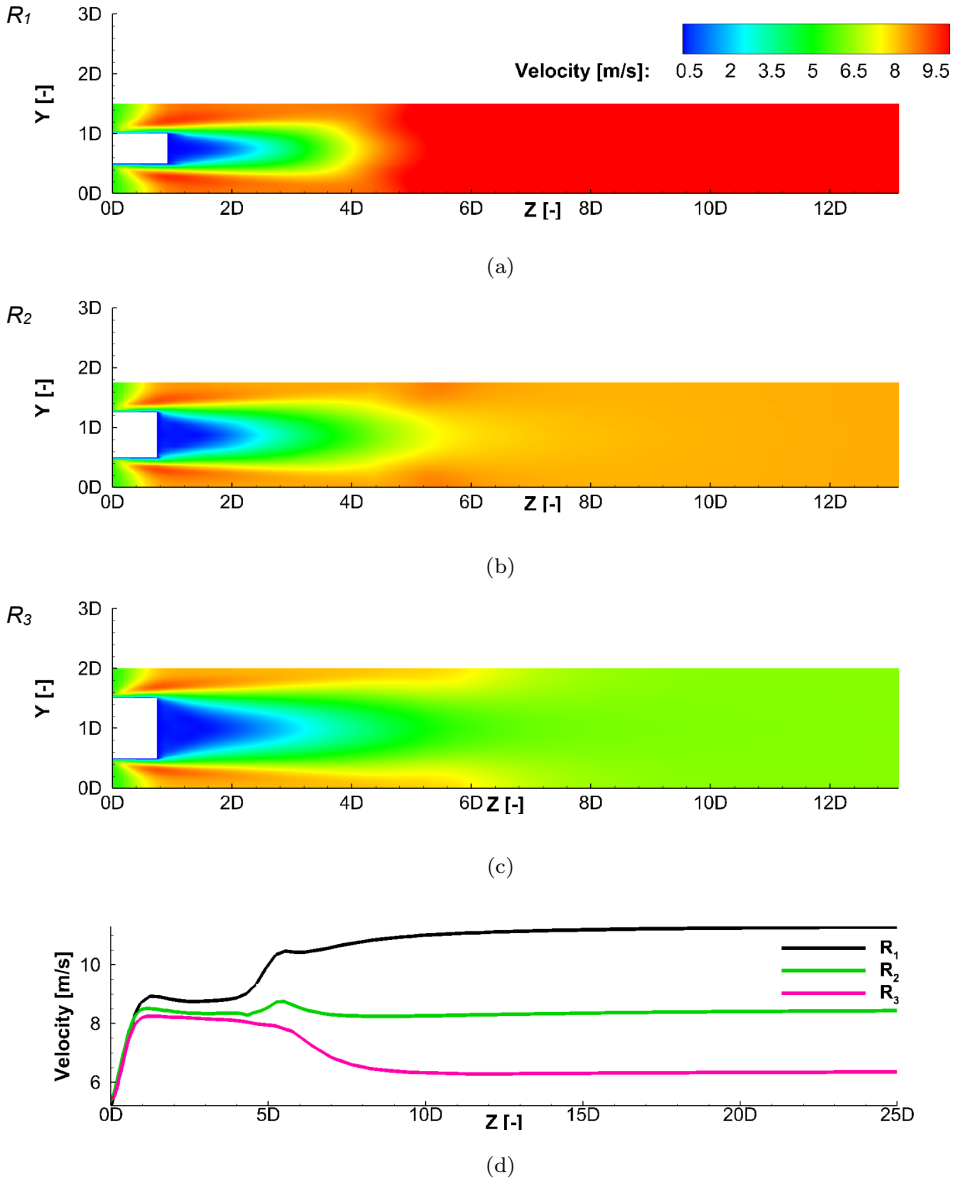

Figure 5: Velocity distribution in the longitudinal plane crossing the axes of two adjacent holes for (a) R_1, (b) R_2, (c) R_3 and (d) velocity profiles along the hole axis. G20 gas.

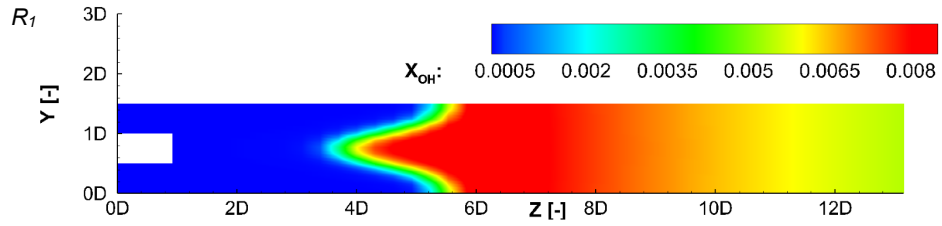

(a)

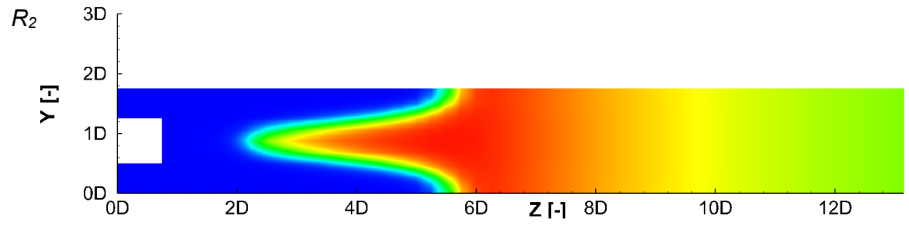

(b)

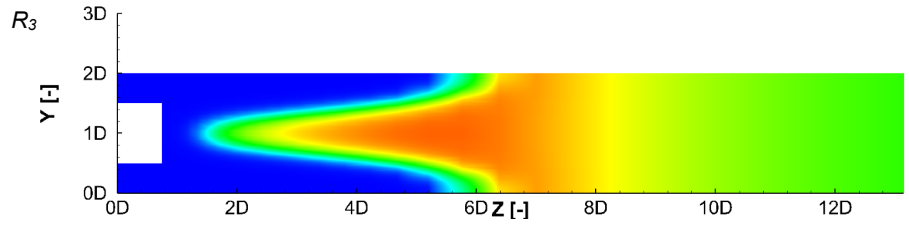

(c)

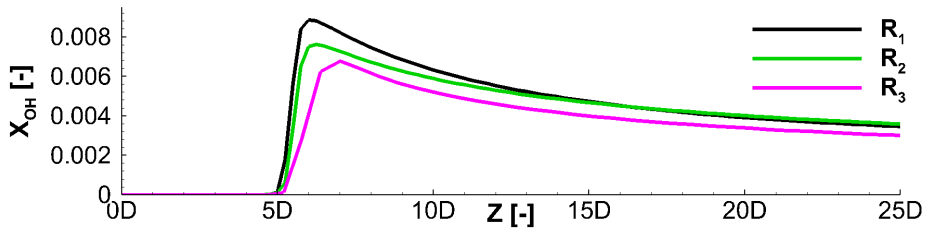

(d)

Figure 6: OH distribution in the longitudinal plane crossing the axes of two adjacent holes for (a) R_1, (b) R_2, (c) R_3 and (d) OH profiles along the hole axis. G20 gas.

To better elucidate the effect of the hole-to-hole distance on the flame characteristics, the temperature distribution in the longitudinal plane crossing the axes of two adjacent holes is shown in Figure 4 for the G20 gas and for the three different R values. With increasing R, the high-temperature region in between two adjacent flames moves towards the burner plate. Subsequently, the thermal field with the largest distance, i.e. R_3 resembles that of a single flame. The downstream temperature slightly decreases with the hole-to-hole distance, as we can observe from the temperature profiles along the flame axis (white line in Figure 2). This behavior can be explained with the increase of the plate surface area with R, which leads to a larger heat transfer rate from the flame to the burner. The temperature profiles along the axis of the hole confirm this trend and highlight the previously mentioned different slope in the reaction zone (see Figure 4), with the flame front moving downstream with increasing R.

Figure 5 shows the flow field for the same G20 gas. We clearly observe the presence of two velocity peaks along the hole axis for both R_1 and R_2 distances. The first peak is due to the gas acceleration triggered by the gas heat up. This velocity peak occurs at $Z \approx 1D$, with some differences related to the different inlet fuel-air flow rates. The second velocity peak takes place immediately downstream of the flame front, at $Z \approx 5.5D$ and its intensity is affected by the hole-to-hole distance. Actually, this second peak is well visible for the smallest hole-to-hole distance, i.e. R_1, while it vanishes for the R_3. Indeed, in such a case the peak is replaced by a change in the slope of the profile. This second peak stems from the interactions between flames as the flow field can be accelerated by the heat transfer from the neighbor

flames. For the largest hole-to-hole distance, such flame interaction is weak, resulting in a small influence on the single-flame behavior.

The reaction zone is illustrated through the distribution of the OH flame marker in Figure 6 fr the G20 gas. The maximum OH concentration is observed for the lowest R value, denoting an intense reaction zone. The OH region moves towards the burner with increasing the hole-to-hole distance; besides, the wavy shape of the OH field is more pronounced with increasing R, thus indicting the trend towards a single premixed flame behavior.

4.2. Effect of H_2 addition

The effect of hydrogen addition on the thermal field is shown in Figure 7, which reports the temperature distribution predicted for the G20, G222 and H2NG mixtures in the R_1 configuration. Increasing the H_2 content in the fuel, the temperature of the flue gases decreases. Indeed, both a decrease in the thermal power and a decrease in the equivalence ratio occur naturally in the domestic boiler with increasing the H_2 content as previously discussed in relation to Table 2. As a consequence, the temperature rise is limited due to both the higher flame dilution and lower thermal load. However, we can also notice anticipation of the flame which is due to the high H_2 reactivity. This behavior is well evident also from the OH field in Figure 8. The OH profile along the hole axis indicates that the peak shifts from $Z = 6D$ to $Z = 5D$ when increasing the H_2 content from 0 to 50%, i.e. from G20 to H2NG mixture. Besides, the flame interaction is less important for the highest H_2 content, with the high-temperature region (see also Figure 7) between the two neighbor flames moving towards the plate. This behavior may be imputed to reduced heat transfer from the neighbor flames stemming from

both the lower thermal load and higher dilution. In particular, the lower equivalence ratio increases the amount of transparent gas and N_2. The flow field, reported in Figure 9 confirms the above observations, with the second velocity peak being imputed to the flame interaction.

The behaviour of the different mixture for the hole-to-hole distance, i.e. R_3, is provided in Figure 10, Figure 11 and Figure 12. The increase in the H_2 content leads to an anticipation of the flame front and a lowering of the flue gas temperature, as already discussed for the R_1 case. However, at first glance, the thermal field is much different than the one with R_1 (see Figure 7) as here the large hole-to-hole distance leads to flames that are well separated between each other. Indeed the high-temperature region between the flames tends to attach to the burner plate.

As for the OH, Figure 11 shows that also for the R_3 case there is a decrease in the OH peak as the H_2 increases due to both the lower thermal load and larger air excess.

Figure 12 shows the velocity distribution at different H_2 content and for the R_3 case: here we notice how the second peak in the velocity profile along the hole axis, already discussed for the lowest hole-to-hole distance, is no more present, and just replaced by a change in the slope of the curve. Indeed a little interaction between neighbor flames occurs for R_3 with just a minor effect on the flow field.

4.3. NO emissions

The effect of both hole-to-hole distance and H_2 content in the fuel on the NO emissions is reported in Table 3. Firstly, we notice how the NO emissions are slightly affected by the hole-to-hole distance. In particular, with

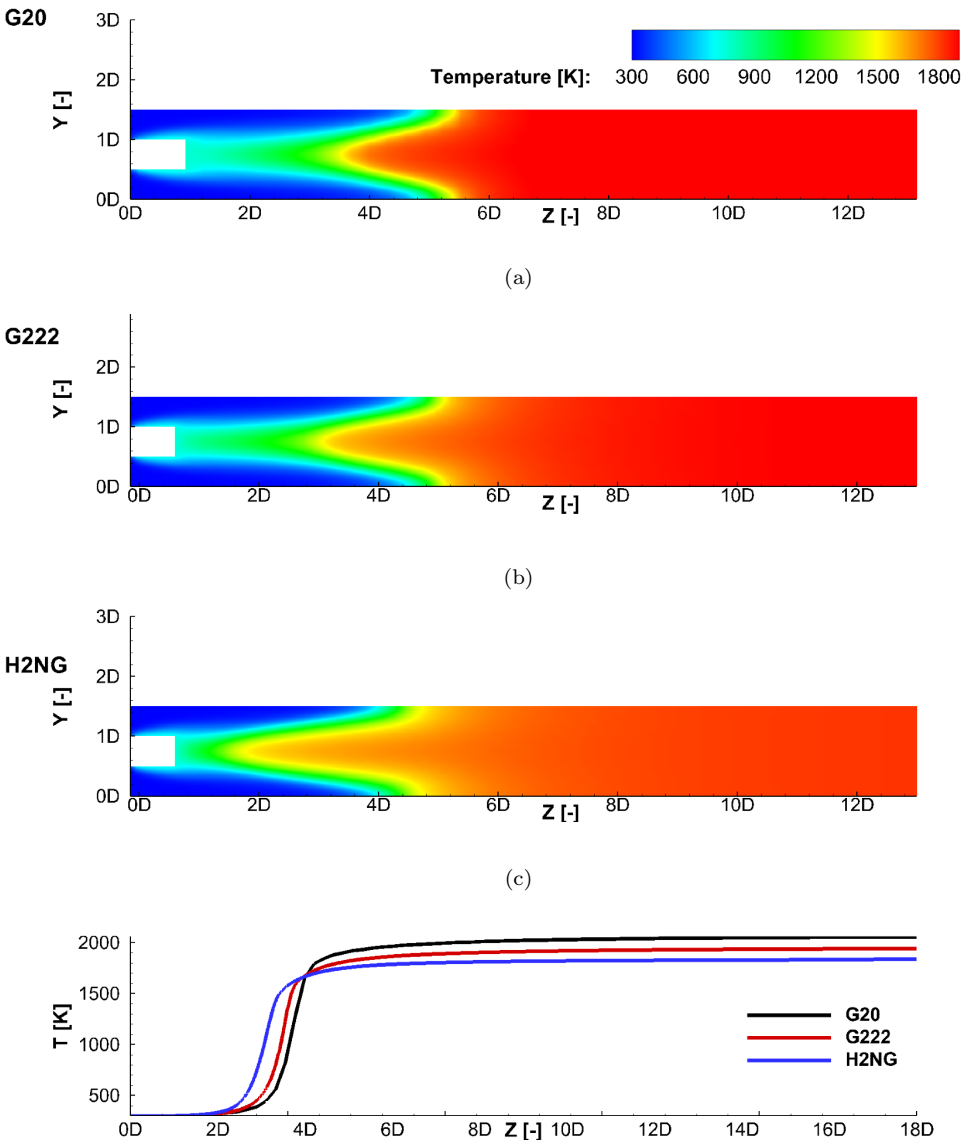

Figure 7: Temperature distribution in the longitudinal plane crossing the axes of two adjacent holes for (a) G20, (b) G222, (c) H2NG and (d) temperature profiles along the hole axis. R_1 configuration.

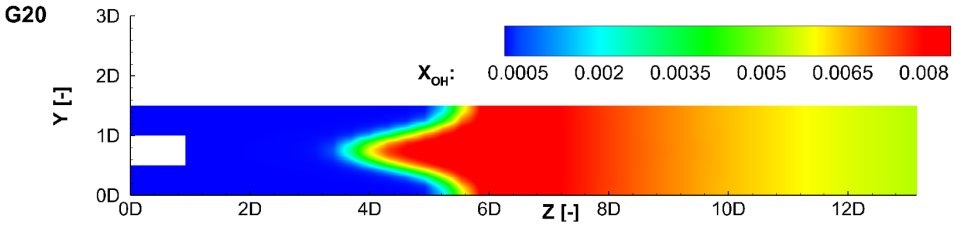

(a)

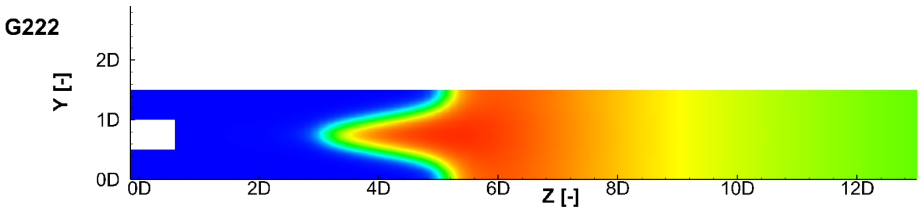

(b)

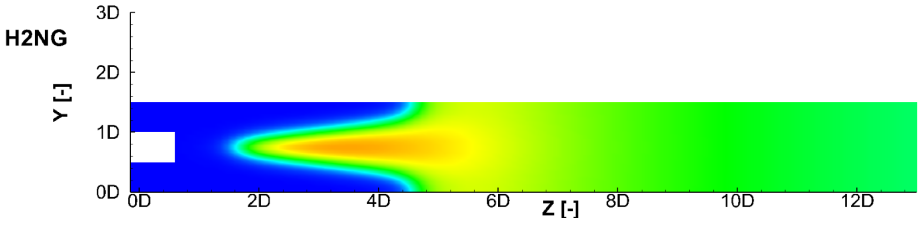

(c)

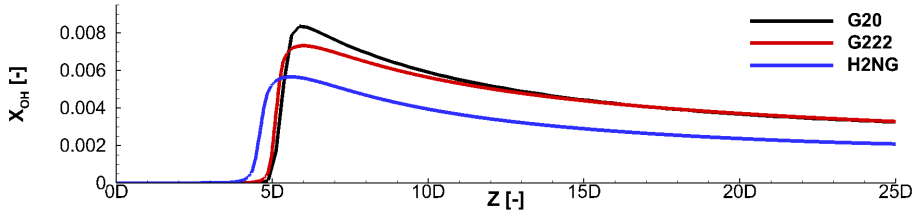

(d)

Figure 8: OH distribution in the longitudinal plane crossing the axes of two adjacent holes for (a) G20, (b) G222, (c) H2NG and (d) OH profiles along the hole axis. R_1 configuration.

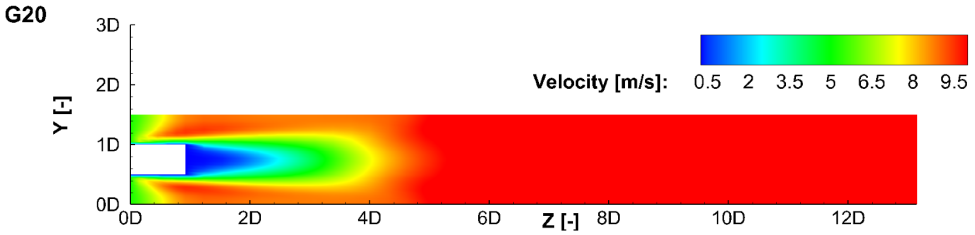

(a)

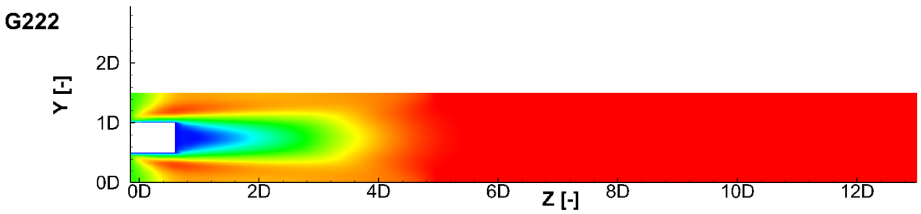

(b)

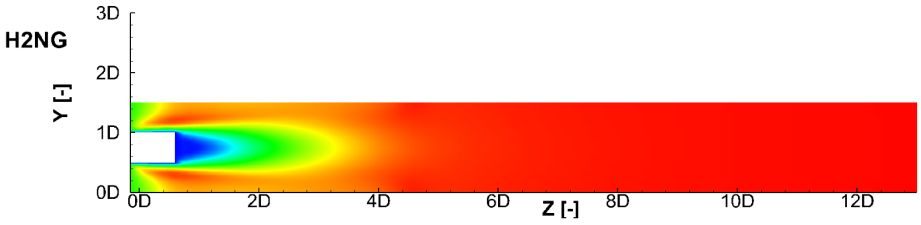

(c)

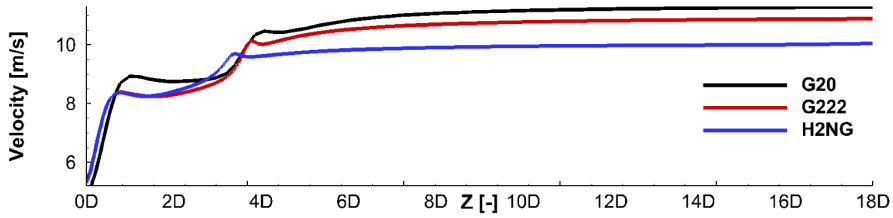

(d)

Figure 9: Velocity distribution in the longitudinal plane crossing the axes of two adjacent holes for (a) G20, (b) G222, (c) H2NG and (d) velocity profiles along the hole axis. R_1 configuration.

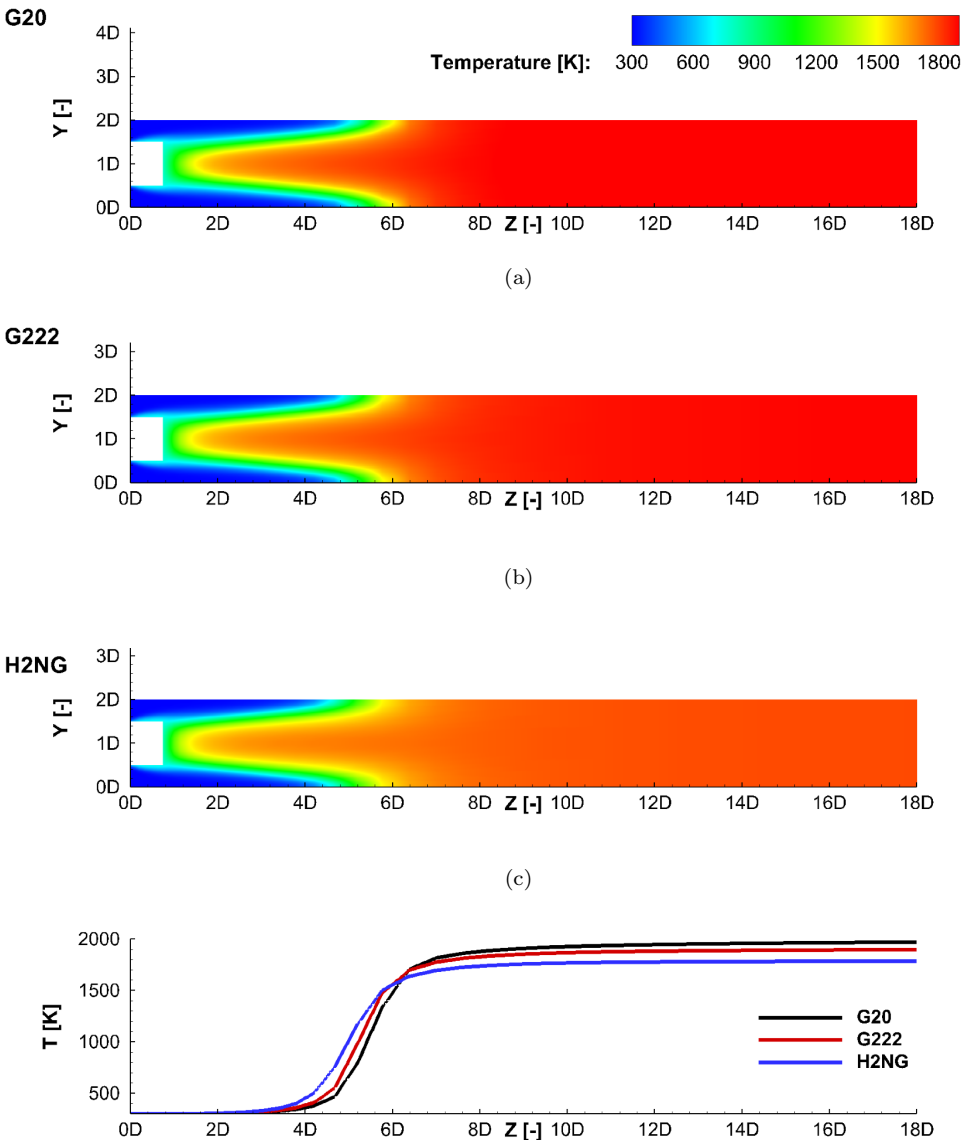

Figure 10: Temperature distribution in the longitudinal plane crossing the axes of two adjacent holes for (a) G20, (b) G222, (c) H2NG and (d) temperature profiles along the hole axis. R_3 configuration.

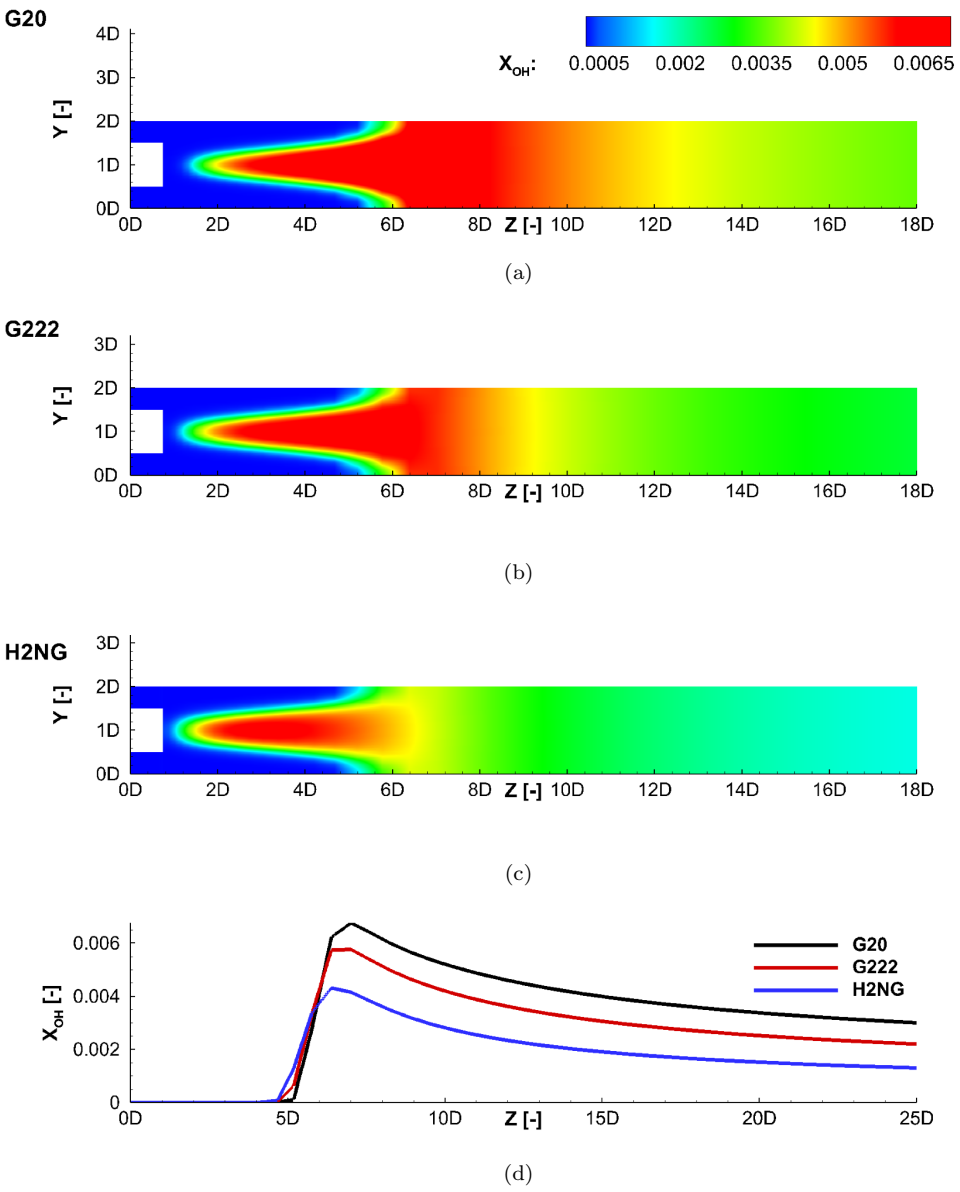

Figure 11: OH distribution in the longitudinal plane crossing the axes of two adjacent holes for (a) G20, (b) G222, (c) H2NG and (d) OH profiles along the hole axis. R_3 configuration.

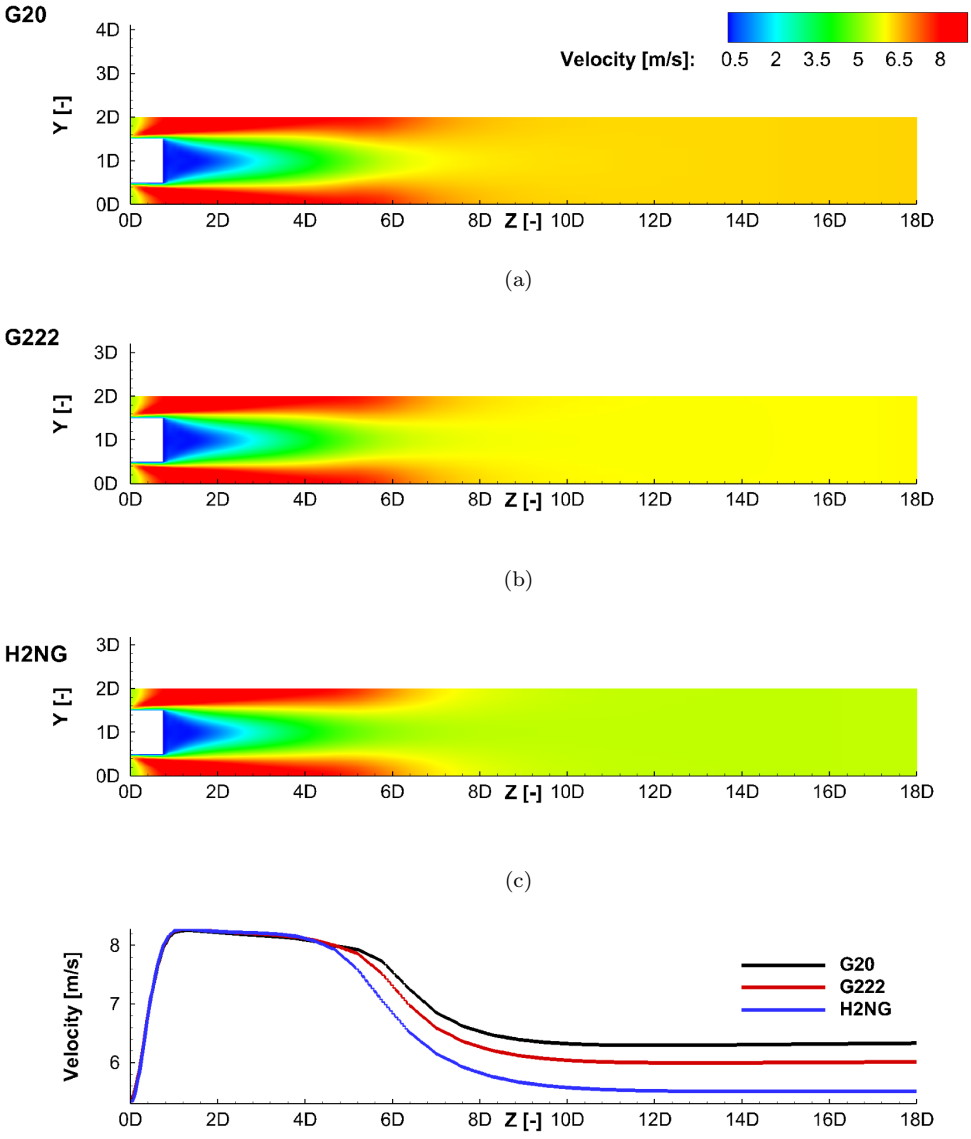

Figure 12: Velocity distribution in the longitudinal plane crossing the axes of two adjacent holes for (a) G20, (b) G222, (c) H2NG and (d) velocity profiles along the hole axis. R_3 configuration.

increasing R the downstream temperature lowers because of the larger heat transfer with the burner plate (see discussion in relation to Figure 4) and, as a consequence, the thermal NO formation route is partially hampered. For instance, the NO emissions decrease from 24 ppm to 22 ppm when moving from R_1 to R_3. This behavior is recurrent for all gas mixtures.

With increasing H_2 content, NO emissions decrease. For instance, for the R_3 case, we observe that NO emissions are suppressed from 22 ppm to 7.5 ppm when changing from the G20 gas to H2NG mixture. To provide a validation of such behaviour, the NO emissions measured in a domestic boiler equipped with the same burner of Figure 1 and operated with the same conditions given in Table 2 are reported in the last column of Table 3. Logically, the burner presents both holes (with a typical pattern as the R_3 configuration) and slits, while the computational model refers just to the portion of the burner, presenting only holes. However, the trend, i.e. the reduction of NO emissions with increasing H_2 content, is confirmed by the experimental data. This behavior can again be explained by the lower temperatures observed with hydrogen stemming from both the smaller thermal load and leaner conditions. Such lower temperatures limit the thermal formation route.

To gain a better insight into the NO formation pathways and on how they are affected by the H_2 content in the fuel, the different contributions to the formation of the total NO were investigated. This analysis was accomplished by performing a first simulation with the full `GRI3.0` mechanism, and subsequently by carrying out additional simulations, each of them by subtracting a specific formation pathway, i.e. the thermal, the N_2O, the prompt and the NNH-intermediate mechanism, from the full `GRI3.0` scheme. In particular

Table 3: Outlet NO values in ppm (dry basis) predicted for different hole-to-hole distances and gas mixtures. Experimental values obtained in a domestic boiler equipped with the burner shown in Figure 1(a) for different gas mixtures.

gas	R_1	R_2	R_3	Exp.
G20	24	23.6	22	20
G222	14.2	13.8	13.8	11
H2NG	7.9	7.7	7.5	5

the NNH-intermediate pathways may be relevant in presence of hydrogen [36, 37]. This procedure and its validation is better described in [38, 39, 40]. Results are reported in Figure 13 for the R_3 distance . We observe an increase of the NNH-intermediate formation and a decrease in the thermal mechanism with increasing the H_2 content in the fuel. In particular, for the H2NG with 50% of H_2, the NNH pathway is responsible for approximately 47.2% of the total NO emissions, while the thermal route for only the 11.2%. Interestingly, significant contributions are due to the prompt and N2O formation pathways. This behaviour is in agreement with the recent work by Hinrichs et al. [24], who carried out 3-D numerical simulations of a single hole of a cylindrical burner fed with the G20 gas test.

5. Conclusion

The effect of hydrogen addition on multi-hole flames emulating portions of multi-hole burners, which are typically encountered in condensing boilers, is analyzed numerically. To this purpose, a preliminary characterization of the impact of the hole-to-hole distance on the flame features is investigated

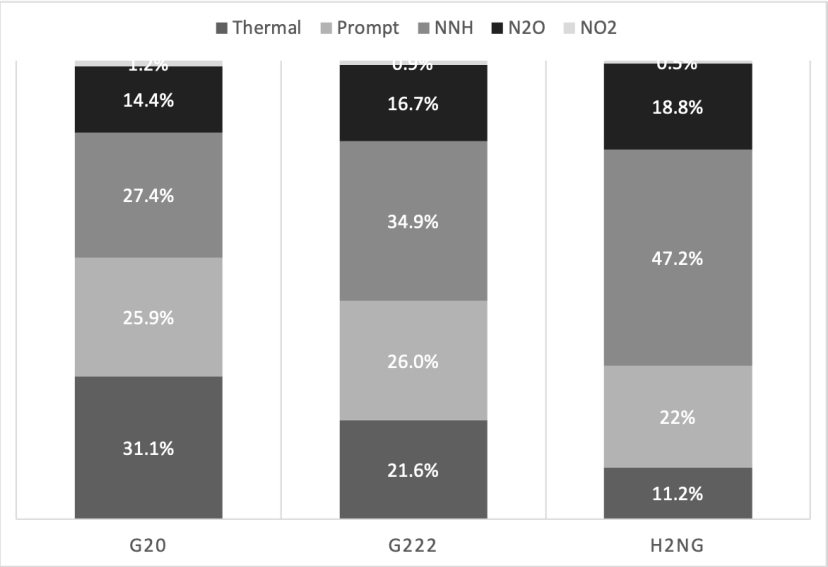

Figure 13: Contribution of NO formation pathways to the the total NO emissions for the different gases. R_3 hole-to-hole distance.

by using practical values of this geometrical parameter. We observe how for small flame distances the flame from a hole interacts with the neighbor flames, while for the largest distances the flames mimic a single-flame behavior. The heat exchange with the burner plate contributes to a decrease of the downstream temperature, which, as a consequence, lowers with increasing R. As for hydrogen addition, a preliminary analysis is carried out to determine the operating conditions that a real condensing boiler achieves when the fuel composition changed from the conventional G20 gas to the H_2-admixtures. This characterization pointed out how the thermal load diminishes, while the boiler operates in leaner conditions, i.e. with a higher amount of air excess. The overall features show that the H_2 addition leads to an anticipation of the flame front towards the burner; however, the larger dilution hampers the

temperature rise. This has a positive impact on the NO emissions. Even though, usually one of the major concerns with the use of hydrogen is the high adiabatic flame temperature that triggers the NO thermal formation, here the natural behavior of the domestic boiler leads to an opposite behavior. Indeed. the higher air excess with H_2-admixtures limits the temperature peaks and suppresses the thermal route with just a few ppm of NO estimated for the 50% H_2 content.

The thermal path represents the dominant contribution to the total NO for the G20 gas, while the reduced temperature for the H2-enriched fuels boost the NNH mechanism. In particular, this pathway is responsible of 47.2% of total NO for the the H2NG gas, with 50% of H_2.

We believe that the coupling between numerical simulations and the analysis of practical operating conditions with H_2 admixtures may help understanding the effect of upcoming variations in gas composition from the distribution network, on the performances of domestic boilers. This may also help devising strategies for limiting pollutant emissions. Logically the problem is more complex and require efforts needed at elucidating also economics [41, 3] and safety aspects [5, 42] related to the H_2 addition in the natural gas network.

Author contributions

Rachele Lamioni: Conceptualization, Methodology, Data curation, Writing-Original draft preparation. Cristiana Bronzoni, Marco Folli and Leonardo Tognotti: Reviewing and Editing. Chiara Galletti: Conceptualization, Methodology, Writing-Original draft preparation.

Acknowledge

This work was supported by the POR FESR 2014-2020 "HyPOWERED" project, funded by Regione Emilia-Romagna, Italy. We also thank Mr. Sebastiano Cinnirella for his help in carrying out numerical simulations.

References

[1] R. McKenna, Q. Bchini, J. Weinand, J. Michaelis, S. König, W. Köppel, W. Fichtner, The future role of power-to-gas in the energy transition: Regional and local techno-economic analyses in baden-württemberg, Applied Energy 212 (2018) 386–400. doi:https://doi.org/10.1016/j.apenergy.2017.12.017.

[2] M. Cavana, A. Mazza, G. Chicco, P. Leone, Electrical and gas networks coupling through hydrogen blending under increasing distributed photovoltaic generation, Applied Energy 290 (2021) 116764. doi:https://doi.org/10.1016/j.apenergy.2021.116764.

[3] C. J. Quarton, S. Samsatli, Should we inject hydrogen into gas grids? practicalities and whole-system value chain optimisation, Applied Energy 275 (2020) 115172. doi:https://doi.org/10.1016/j.apenergy.2020.115172.
URL https://www.sciencedirect.com/science/article/pii/S030626192030684X

[4] F. Cell, H. J. Undertaking, Hydrogen roadmap europe: A sustainable pathway for the european energy transition, Hydrogen Knowledge Centre (2019).

[5] F. Schiro, A. Stoppato, A. Benato, Modelling and analyzing the impact of hydrogen enriched natural gas on domestic gas boilers in a decarbonization perspective, Carbon Resources Conversion 3 (2020) 122–129. doi:https://doi.org/10.1016/j.crcon.2020.08.001.

[6] S. Carpentier, P. Milin, N. Mostefaoui, P. Nitschke-Kowsky, J. Schweitzer, Negar Sadegh, O. Thibaut, Self-regulated gas boilers able to cope with gas quality variation state of the art and performances.
URL https://www.gerg.eu/wp-content/uploads/2019/10/CCCB_Report_final.pdf

[7] Q. Chen, K. Finney, H. Li, X. Zhang, J. Zhou, V. Sharifi, J. Swithenbank, Condensing boiler applications in the process industry, Applied Energy 89 (1) (2012) 30–36. doi:https://doi.org/10.1016/j.apenergy.2010.11.020.

[8] F. Schiro, A. Stoppato, Experimental investigation of emissions and flame stability for steel and metal fiber cylindrical premixed burners, Combustion Science and Technology 191 (3) (2019) 453–471. doi:https://doi.org/10.1080/00102202.2018.1500556.

[9] S. Lee, S.-M. Kum, C.-E. Lee, An experimental study of a cylindrical multi-hole premixed burner for the development of a condensing gas boiler, Energy 36 (7) (2011) 4150–4157. doi:https://doi.org/10.1016/j.energy.2011.04.029.

[10] M. Najarnikoo, M. Z. Targhi, H. Pasdarshahri, Experimental study on

the flame stability and color characterization of cylindrical premixed perforated burner of condensing boiler by image processing method, Energy 189 (2019) 116130. doi:10.1016/J.ENERGY.2019.116130.

[11] H. Soltanian, M. Z. Targhi, H. Pasdarshahri, Chemiluminescence usage in finding optimum operating range of multi-hole burners, Energy 180 (2019) 398–404. doi:10.1016/j.energy.2019.05.104.

[12] Y. Ding, D. Durox, N. Darabiha, T. Schuller, Chemiluminescence of Burner-Stabilized Premixed Laminar Flames, Combustion Science and Technology (1) 18–42. doi:10.1080/00102202.2018.1558391.

[13] H. J. Burbano, A. A. Amell, J. M. García, Effects of hydrogen addition to methane on the flame structure and co emissions in atmospheric burners, International Journal of Hydrogen Energy 33 (13) (2008) 3410–3415. doi:https://doi.org/10.1016/j.ijhydene.2008.04.020.

[14] D.-F. Zhao, F.-G. Liu, X.-Y. You, R. Zhang, B.-L. Zhang, G.-L. He, Optimization of a premixed cylindrical burner for low pollutant emission, Energy Conversion and Management 99 (2015) 151–160. doi:https://doi.org/10.1016/j.enconman.2015.04.039.

[15] T.-H. Zhang, F.-G. Liu, X.-Y. You, Optimization of gas mixing system of premixed burner based on cfd analysis, Energy Conversion and Management 85 (2014) 131–139. doi:10.1016/J.ENCONMAN.2014.05.055.

[16] M. H. Saberi Moghaddam, M. Saei Moghaddam, M. Khorramdel, Numerical study of geometric parameters effecting temperature and ther-

mal efficiency in a premix multi-hole flat flame burner, Energy 125 (2017) 654–662. doi:10.1016/j.energy.2017.02.116.

[17] G. Hassan, M. Pourkashanian, D. Ingham, L. Ma, S. Taylor, Reduction in pollutants emissions from domestic boilers—computational fluid dynamics study, Journal of Thermal Science and Engineering Applications 1 (1). doi:https://doi.org/10.1115/1.3159526.

[18] H. M. Altay, K. S. Kedia, R. L. Speth, A. F. Ghoniem, Two-dimensional simulations of steady perforated-plate stabilized premixed flames, Combustion Theory and Modelling 14 (1) (2010) 125–154. doi:10.1080/13647831003660859.

[19] K. S. Kedia, A. F. Ghoniem, Mechanisms of stabilization and blowoff of a premixed flame downstream of a heat-conducting perforated plate, Combustion and Flame (3) 1055–1069. doi:10.1016/j.combustflame.2011.10.014.

[20] E. V. Jithin, V. R. Kishore, R. J. Varghese, Three-dimensional simulations of steady perforated-plate stabilized propane-air premixed flames, Energy and Fuels 28 (8) (2014) 5415–5425. doi:10.1021/ef401903y.

[21] J. Edacheri Veetil, B. Aravind, A. Mohammad, S. Kumar, R. K. Velamati, Effect of hole pattern on the structure of small scale perorated plate burner flames, Fuel 216 (2018) 722–733. doi:10.1016/J.FUEL.2017.12.057.

[22] R. Lamioni, P. E. Lapenna, L. Berger, K. Kleinheinz, A. Attili, H. Pitsch, F. Creta, Pressure-induced hydrodynamic instability in

premixed methane-air slot flames, Combustion Science and Technology 192 (11) (2020) 1998–2009. doi:https://doi.org/10.1080/00102202.2020.1768081.

[23] A. Attili, R. Lamioni, L. Berger, K. Kleinheinz, P. E. Lapenna, H. Pitsch, F. Creta, The effect of pressure on the hydrodynamic stability limit of premixed flames, Proceedings of the Combustion Institute 38 (2) (2021) 1973–1981. doi:https://doi.org/10.1016/j.proci.2020.06.091.

[24] J. Hinrichs, D. Felsmann, S. Schweitzer-De Bortoli, H.-J. Tomczak, H. Pitsch, Numerical and experimental investigation of pollutant formation and emissions in a full-scale cylindrical heating unit of a condensing gas boiler, Applied Energy 229 (2018) 977–989. doi:10.1016/j.apenergy.2018.08.011.

[25] A. Cuoci, A. Frassoldati, T. Faravelli, E. Ranzi, Opensmoke++: An object-oriented framework for the numerical modeling of reactive systems with detailed kinetic mechanisms., Computer Physics Communications. 192 (2015) 237–264. doi:https://doi.org/10.1016/j.cpc.2015.02.014.

[26] T. Aizawa, Diode-laser wavelength-modulation absorption spectroscopy for quantitative in situ measurements of temperature and oh radical concentration in combustion gases, Applied Optics 40 (27) (2001) 4894–4903. doi:https://doi.org/10.1364/AO.40.004894.

[27] P. Cheng, Two-dimensional radiating gas flow by a moment method,

AIAA Journal 2 (9) (1964) 1662–1664. doi:https://doi.org/10.2514/3.2645.

[28] R. Siegel, J. R. Howell, Thermal radiation heat transfer, hemisphere pub, Corp., Washing ton DC.

[29] T. F. Smith, Z. F. Shen, J. N. Friedman, Evaluation of coefficients for the weighted sum of gray gases model, Journal of Heat Transfer 104 (4) (1982) 602–608. doi:10.1115/1.3245174.

[30] T. Poinsot, D. Veynante, Theoretical and numerical combustion, RT Edwards, Inc., 2005.

[31] H. de Vries, A. V. Mokhov, H. B. Levinsky, The impact of natural gas/hydrogen mixtures on the performance of end-use equipment: Interchangeability analysis for domestic appliances, Applied Energy 208 (2017) 1007–1019. doi:https://doi.org/10.1016/j.apenergy.2017.09.049.

[32] J. Hinrichs, S. Schweitzer-De Bortoli, H. Pitsch, 3D modeling framework and investigation of pollutant formation in a condensing gas boiler, Fuel 300 (2021) 120916. doi:https://doi.org/10.1016/j.fuel.2021.120916.

[33] N. Beishuizen, D. Mayer, Conjugate heat transfer simulations of perforated plate burners using flamelet generated manifolds.

[34] A. Fluent, et al., 12.0 user's guide, Ansys Inc 6.

[35] E. C. Okafor, A. Hayakawa, Y. Nagano, T. Kitagawa, Effects of hydrogen concentration on premixed laminar flames of hydrogen–methane–air, International Journal of Hydrogen Energy 39 (5) (2014) 2409–2417. doi:https://doi.org/10.1016/j.ijhydene.2013.11.128.

[36] C. Galletti, A. Parente, M. Derudi, R. Rota, L. Tognotti, Numerical and experimental analysis of no emissions from a lab-scale burner fed with hydrogen-enriched fuels and operating in mild combustion, International Journal of Hydrogen Energy 34 (19) (2009) 8339–8351. doi:10.1016/j.ijhydene.2009.07.095.

[37] A. Parente, C. Galletti, L. Tognotti, A simplified approach for predicting no formation in mild combustion of ch4–h2 mixtures, Proceedings of the Combustion Institute 33 (2) (2011) 3343–3350. doi:https://doi.org/10.1016/j.proci.2010.06.141.

[38] F. Guethe, M. de la Cruz Garcià, A. Burdet, Flue gas recirculation in gas turbine: Investigation of combustion reactivity and nox emission, Vol. 48838, 2009, pp. 179–191. doi:10.1115/GT2009-59221.

[39] P. Trisjono, H. Pitsch, A direct numerical simulation study on no formation in lean premixed flames, Proceedings of the Combustion Institute 36 (2) (2017) 2033–2043. doi:https://doi.org/10.1016/j.proci.2016.06.130.

[40] E.-S. Cho, S. Chung, Numerical evaluation of nox mechanisms in methane-air counterflow premixed flames, Journal of Mechanical Sci-

ence and Technology 23 (3) (2009) 659–666, cited By 9. doi:10.1007/s12206-008-1222-y.

[41] A. Lewandowska-Bernat, U. Desideri, Opportunities of power-to-gas technology in different energy systems architectures, Applied energy 228 (2018) 57–67.

[42] L. de Santoli, R. Paiolo, G. Lo Basso, An overview on safety issues related to hydrogen and methane blend applications in domestic and industrial use, Energy Procedia 126 (2017) 297–304, aTI 2017 - 72nd Conference of the Italian Thermal Machines Engineering Association. doi:https://doi.org/10.1016/j.egypro.2017.08.224.
URL https://www.sciencedirect.com/science/article/pii/S187661021733730X